AIAA SciTech Forum
6-10 January 2025, Orlando, FL
AIAA SCITECH 2025 Forum

10.2514/6.2025-1551

Additively Manufactured Spinodal Metamaterials for Aerospace Systems: A Data-Driven Design Framework

Saltuk Yıldız*, Zekeriya Ender Eğer†, and Pınar Acar‡
Virginia Tech, Blacksburg, 24061, VA, USA

Spinodal shapes are composed of smooth structural formations. With their unique topology, they can demonstrate enhanced mechanical behavior with low stress concentrations in comparison to conventional truss and surface-based metamaterials. In this work, a computational and data-driven design study is carried out to find the optimum design parameters of additively manufactured 2D spinodal metamaterials made of the Ti-6Al-4V alloy to improve their mechanical performance for aerospace systems. In the proposed approach, 2D spinodal systems are computationally designed by the parameterization of the orientation space. Static structural finite element (FE) simulations are performed to compute their energy fraction (E_f) values, quantitatively representing the stress/strain distributions over domain area, which are then compared to the common truss-based lattice cells having the same relative densities. The strain energy density function is calculated by incorporating tensile and shear deformations. An optimization problem is formulated to minimize a composite objective function comprising maximum and average energy fractions higher than a threshold value. The optimization problem is solved with the pattern search algorithm using the physics-based framework, as well as a deep-learning-based surrogate model. The optimum design is expected to reveal the prospective use of spinodal systems in aerospace structures requiring high mechanical performance.

Nomenclature

β	=	number of waves
σ_{ij}	=	stress tensor
ε_{ij}	=	strain tensor
θ	=	cone angle
η_m	=	orientation distribution
ν_{ij}	=	Poisson's ratio
γ_m	=	phase angle
ϕ_0	=	threshold porosity
$\psi(x)$	=	local phase field function
E	=	modulus of elasticity
E_f	=	energy fraction
W_e	=	strain energy density
W_{total}	=	total strain energy density
d_{rel}	=	relative density
m	=	wave vector
M	=	number of cosine waves
t	=	layer thickness
u_{ii}	=	normal displacement
u_{ij}	=	shear displacement
$X(x)$	=	binary indicator function

*Graduate Research Assistant, Ph.D. Student, Department of Mechanical Engineering, AIAA Student Member
†Graduate Research Assistant, Ph.D. Student, Department of Mechanical Engineering, AIAA Student Member
‡Associate Professor, Department of Mechanical Engineering, AIAA Member

I. Introduction

In recent years, metamaterials with complex shapes have gained popularity owing to the developments in advanced manufacturing techniques allowing the manufacturing of lightweight structures with high strength-to-weight ratios desired for aerospace applications [1]. The conventional metamaterials composed of trusses or surfaces with sharp geometric features are subject to high-stress accumulations and undesired local mechanical failures [2]. For improved mechanical behavior, a novel type of metamaterials called spinodal metamaterials has been proposed by Kumar et al. [3]. These materials consist of wavy surfaces and smooth transitions between topological features resulting in low stress concentrations while satisfying high-stiffness and low-density requirements. This type of material system has originated from the separation of two or more phases [4]. Kumar et al. [3] solved an inverse problem to generate 3D anisotropic and functionally graded spinodal topologies as bio-inspired natural bone structures. For this purpose, they presented a data-driven design framework predicting desired anisotropic stiffness values. Zheng et al. [5] developed a surrogate model utilizing a deep neural network to extract homogenized elastic properties of the spinodal microstructures to solve a multi-scale topology optimization problem. After the preliminary examinations of these novel metamaterials, investigating their property-structure (PS) linkage through deep-learning methods has become a prominent research topic in the current literature. For this purpose, Mao et al. [6] studied the PS linkage of spinodal microstructures using generative adversarial networks (GAN) and mixture density networks (MDN) to compute their optical properties. Röding et al. [7] have followed a similar approach using a convolutional neural network (CNN) algorithm targeting the mass transport property of 3D spinodal metamaterials. Golnary and Asghari [8] determined the linkage between anisotropic material properties and design inputs with the help of unsupervised machine learning.

Spinodal systems with metallic base materials can be additively manufactured. However, there are limited studies on additive manufacturing and experimental testing of spinodal metamaterials in the literature [9–12]. Thakolkaran et al. [9] experimentally investigated the mechanical behavior of spinodal materials having large deformations through compression tests and they developed a particle input convex neural network (PICNN) model trained by experimental data. Most of the studies analyze polymer base materials for spinodal systems and thus investigating metallic spinodal systems is still a gap in the literature. Vafaeefar et al. [10] also analyzed elastic responses of spinodal structures and compared them with triply periodic minimal surface (TPMS) systems such as gyroid and truss-based metamaterials. Later on, they experimentally and numerically extracted energy absorption properties of 3D-printed spinodal metamaterials made of polymer base materials through explicit finite element analysis (FEA) and uni-axial compression tests, and their energy absorption performance was compared with conventional surface and truss-based materials [12]. Although truss-based metamaterials demonstrate impressive energy absorption behavior, they may show undesired deformation/failure behavior due to sharp geometric properties [13]. The superiority of spinodal metamaterials is not only their mechanical performance but also their acoustics properties. For this respect, Wojciechowski et al. [11] tested the sound absorption behavior of additively manufactured (i.e., fused filament fabrication (FFF)) spinodal materials having isotropic, cubic, columnar, and lamellar architectures using two-microphone impedance tube test technique and they mathematically determined bulk properties using Johnson Champoux-Allard theory.

Recently, the homogenized elastic properties of the spinodal metamaterials made of ULTEM 1000 polymer have been extracted and 2D systems have been inversely designed through generative adversarial networks (CGAN) by Liu and Acar [14]. However, the spinodal systems made of titanium alloys, which are commonly used for aerospace applications, have not been investigated in the literature to the best of the authors' knowledge.

In this work, the spinodal geometries are generated using the Gaussian Random Field (GRF) approach without expensive time-dependent computations. An additively manufactured titanium-aluminum alloy (Ti-6Al-4V) is selected as a base material. The FE simulations are performed assuming that the metamaterial is under shear and tensile loading. The energy fraction values of each design sample are calculated by conducting static structural simulations. By means of the proposed approach, the optimal values of two sets of orientation distributions (η) defining the unit cell topology are determined to minimize the maximum energy and average energy fraction values. The design strategy involves deep-learning-based optimization with the use of the pattern search method [15]. The mechanical performance of the spinodal materials is also compared with the conventional lattice structures, which are selected from the pool of existing configurations in the literature. Since the spinodal materials have smooth topologies, their effectiveness over conventional systems is discussed in depth.

The outline of this study can be drawn as follows. In Section 2, the computational design of spinodal metamaterials and the numerical approach including meshing, and the definition of boundary conditions and elastic material model are presented. In the following section, the deep-learning-based and conventional optimization approaches are summarized, and exemplary FE results are presented for sample optimum designs with comparison to truss-based metamaterials.

II. Methodology

A. Computational generation of spinodal metamaterials

The spinodal metamaterial designs are derived through spinodal decomposition determining the phase field using the Gaussian Random Field (GRF). The phase field function mathematically represents the physical solid phase of a spinodal structure and can be calculated using Eq. (1) [3].

$$\psi(x) = \sqrt{\frac{2}{M}} \sum_{m=1}^{M} \cos(\beta \eta_m \cdot x + \gamma_m) \tag{1}$$

In Eq. (1), the solid phase field of the spinodal cell is described by M number of cosine waves, non-zero constant number of waves (β), the orientation of the uniform distribution (η_m), and the phase angle (γ_m).

$$\eta_m \sim U\left(\left\{k \in S^2 : (|k \cdot \hat{e}_1| > \cos(\theta_1)) \oplus (|k \cdot \hat{e}_2| > \cos(\theta_2))\right\}\right) \tag{2}$$

In Eq. (2), the randomized cone angles (θ_1, θ_2) determine the final spinodal phases. In the proposed computational design framework, these angles are randomized between 15^o and 90^o. Moreover, the number of cosine waves (M) and constant wave number (β) are selected as 3 and 6π, respectively. The threshold porosity is kept at 0.35, and the relative density (d_{rel}) of each geometry is 60%.

In the computational design framework, a small frame is generated outside the border of the spinodal unit cell to prevent connection loss between the periodic adjacent cells. These metamaterials can be used as internal structures of aircraft due to their lightweight and impressive mechanical behavior in the future. The general design of a spinodal metamaterial as an aerospace structure is illustrated in Fig. 1.

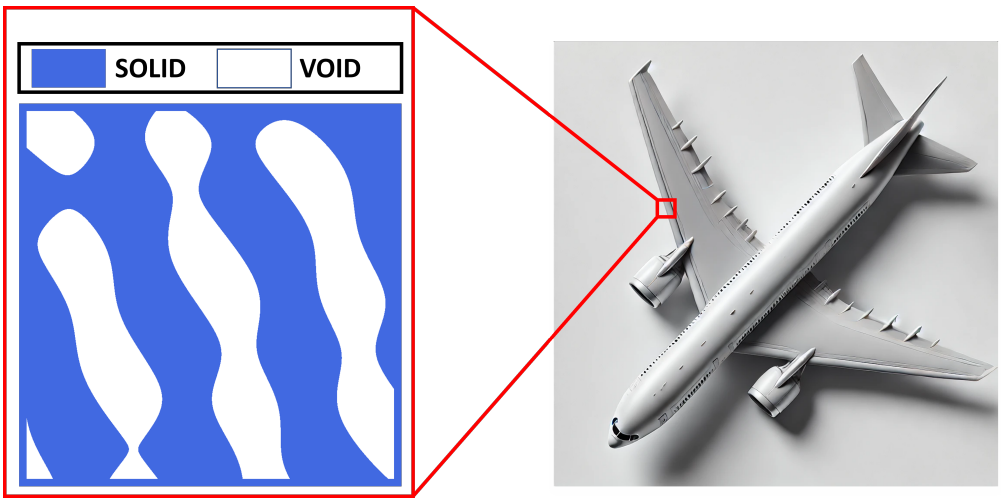

Fig. 1 The phases of a spinodal metamaterial (The airplane image is generated via AI text-to-image generator DALL-E [16]).

In Ref. [17], the phase field is mathematically depicted with a binary indicator as follows:

$$X(x) = \begin{cases} \text{if } \psi(x) \leq \phi_0 & 1 \\ \text{else} & 0 \end{cases} \tag{3}$$

In Eq. (3), if the phase field is lower and equal to the threshold porosity, the domain is defined as solid. If not, it is void as also seen in Fig. 1. According to the aforementioned computational design approach, multiple spinodal metamaterials are generated as gray-scale 2D images depicted in Fig. 2.

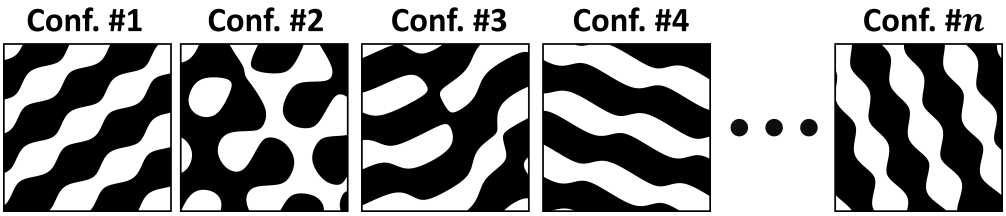

Fig. 2 Randomly generated spinodal metamaterial configurations.

The corresponding orientation distribution sets for each design illustrated in Fig. 2, are listed in 1.

Table 1 Normalized values of orientation distributions for sample spinodal metamaterials shown in Fig. 2.

Configuration #	η_{m_1}	η_{m_2}
1	[-0.60616, 0.71781, 0.60597]	[-0.79534, -0.69624, 0.79549]
2	[0.81587, 0.21152, 0.89037]	[0.57824, 0.97737, -0.45525]
3	[0.28305, 0.014479, 0.82347]	[0.95911, 0.9999, 0.56735]
4	[0.29528, -0.26271, 0.87054]	[-0.95541, 0.96487, -0.4921]
n-1	. . . . .	. . . . .
n	[0.95422, -0.93231, -0.29017]	[-0.2991, 0.36165, -0.95698]

B. Material model

In this computational design and simulation framework, Ti-6Al-4V alloy is utilized as a base material, which is manufactured through the selective laser melting (SLM) method. The experimental data, extracted by testing a dog-bone specimen in Refs. [18, 19], is listed in Table 2.

Table 2 Elastic properties of an additively manufactured Ti-6Al-4V [18, 19].

Property	Value
Modulus of elasticity, E (in GPa)	110
Poisson's ratio, ν_{12}	0.3

C. Numerical simulation

In this section, the principle stresses and strains are obtained from FEA in normal and transverse directions. The values in the z direction are excluded due to the plane stress assumption. The strain energy density (W_e) is determined for each element as given in Eq. (4).

$$W_e = \frac{1}{2}\sum_{i=1}^{2}\sum_{j=1}^{2}\sigma_{ij}\cdot\varepsilon_{ij} \tag{4}$$

In Eq. (4), σ_{ij} and ε_{ij} demonstrate normal and shear stress and strain components, respectively. After obtaining strain energy densities, the energy fractions (E_f) are calculated by dividing the strain energy density by the total strain energy density (i.e., summation of elemental strain energy densities, denoted as W_{total} in Eq. (5)) as shown in Eq. (6).

$$W_{total} = \sum_{e=1}^{N} W_e \tag{5}$$

$$E_f = W_e / W_{total} \tag{6}$$

The spinodal materials are designed and saved as binary images. Later on, im2mesh function [20], which creates high-quality meshes and captures the complex locations, is used to generate triangular elements on spinodal shapes. The three-node plane stress element (CPS3) is used as an element type enabling convergence of the numerical simulation. An example mesh generated for a spinodal material is shown in Fig. 3. In this study, static structural FEA is performed using the commercial software ABAQUS/Standard.

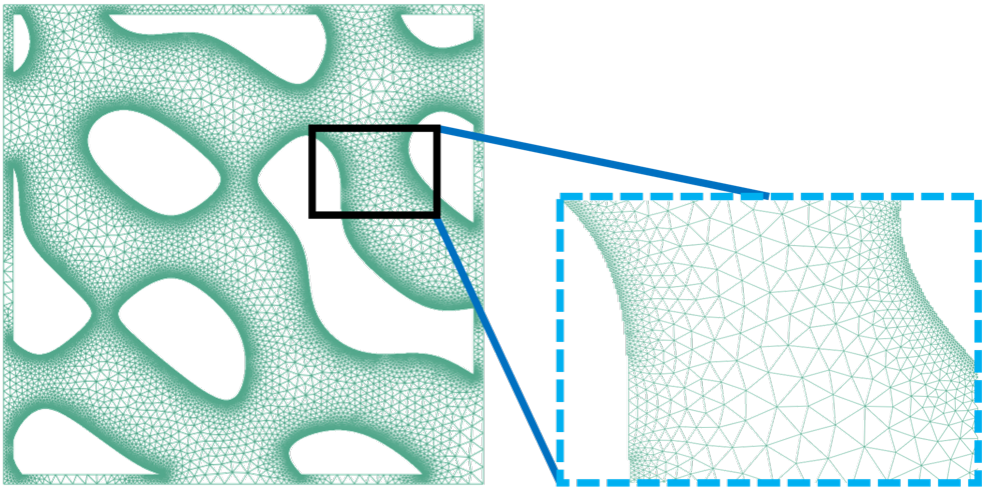

Fig. 3 FE mesh generation and detailed triangular mesh view.

The metamaterials are simulated under shear and tension. The axial tension and shear is defined through the displacement (u_{ii} and u_{ij}) that is equal to 20% of the side length of the unit cell. The boundary conditions defined in the FEA are demonstrated in Fig. 4. The linear elastic properties of an additively manufactured Ti-6Al-4V alloy given in Table 2 are utilized as the linear-elastic material model.

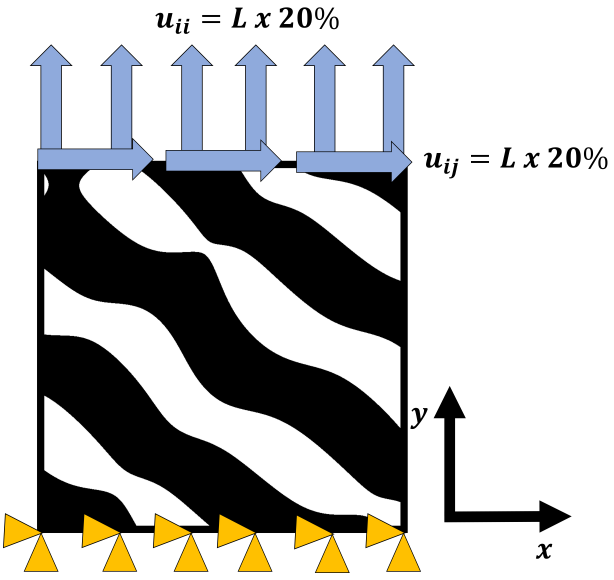

Fig. 4 Boundary and loading conditions defined for a spinodal unit cell.

III. Results & Discussions

A. Surrogate model development and optimization

In this part, deep-learning-based (DL-based) and derivative-free optimization problems are constructed to determine the optimum design of spinodal metamaterials to minimize the maximum and average energy fractions of the elements. The orientation distributions are defined as input design parameters. The DL-based framework is trained with 400 data samples, where the orientation distributions along x and y directions in the cartesian coordinate system are selected as input, while maximum and average energy fraction data are selected as outputs. Next, an objective function is derived through these two outputs and the constrained optimization problem is solved by utilizing the DL-based approach. A gradient-free search algorithm is used to verify the DL-based approach. The mathematical formulation of this optimization problem is given as:

$$\begin{aligned} &\text{minimize} && E_{f_{avg.}} + \zeta x E_{f_{max.}} \\ &\text{find`} && \boldsymbol{\eta}_{mx2} \\ &\text{subject to} && \theta_1 = 15^o, \theta_2 = 90^o \end{aligned} \tag{7}$$

where $E_{f_{avg.}}$ is average energy fraction above threshold and $E_{f_{max.}}$ stands for the maximum energy fraction that is multiplied by a constant ζ. The optimal orientation distributions η_{mx2} are determined within the cone angle constraints (θ_1 and θ_2).

The feed-forward neural network (FNN) based surrogate model and optimization framework are demonstrated in Fig. 5

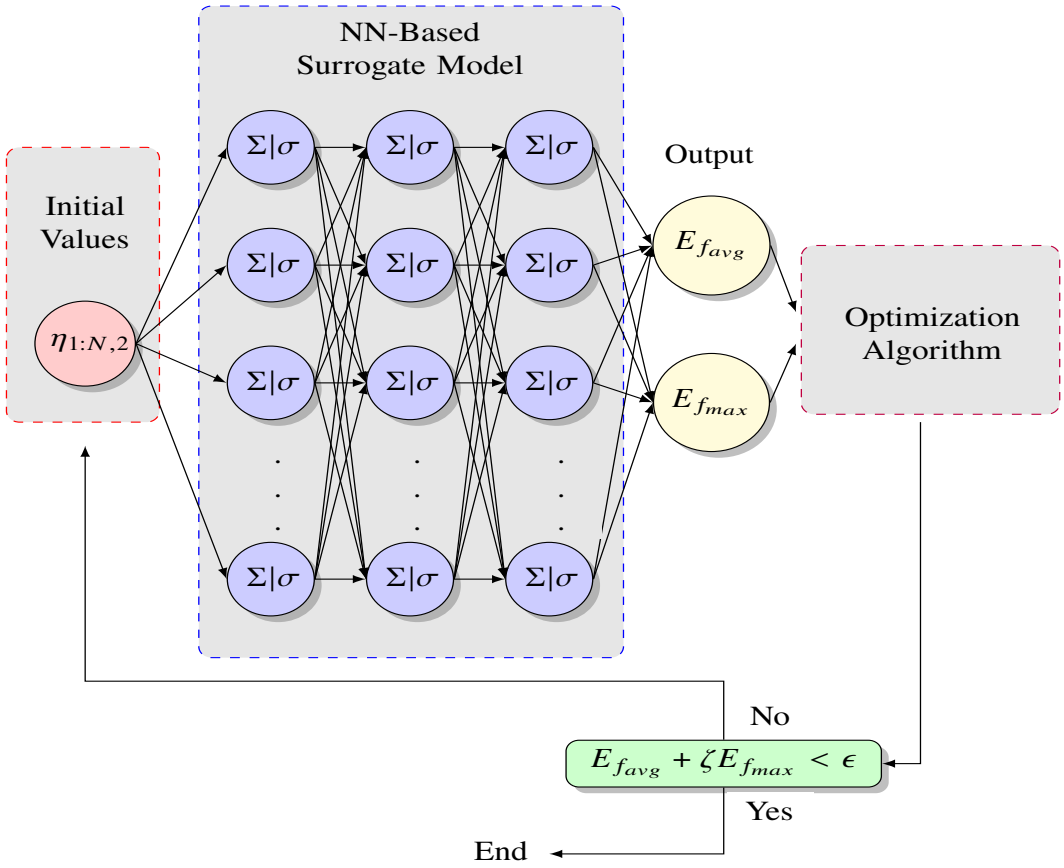

Fig. 5 Schematic of the surrogate model framework. The network will be trained with the variables in the design space to predict the $E_{f_{avg.}}$ and $E_{f_{max.}}$ parameter and then used to minimize its value.

As seen in Fig. 6, 8 different baseline configurations, where the orientations are uniformly distributed between 15^o

and 45^o cone angles, are simulated. The minimum average energy fraction is calculated for the 7^{th} configuration (Fig. 6) is selected as the threshold value.

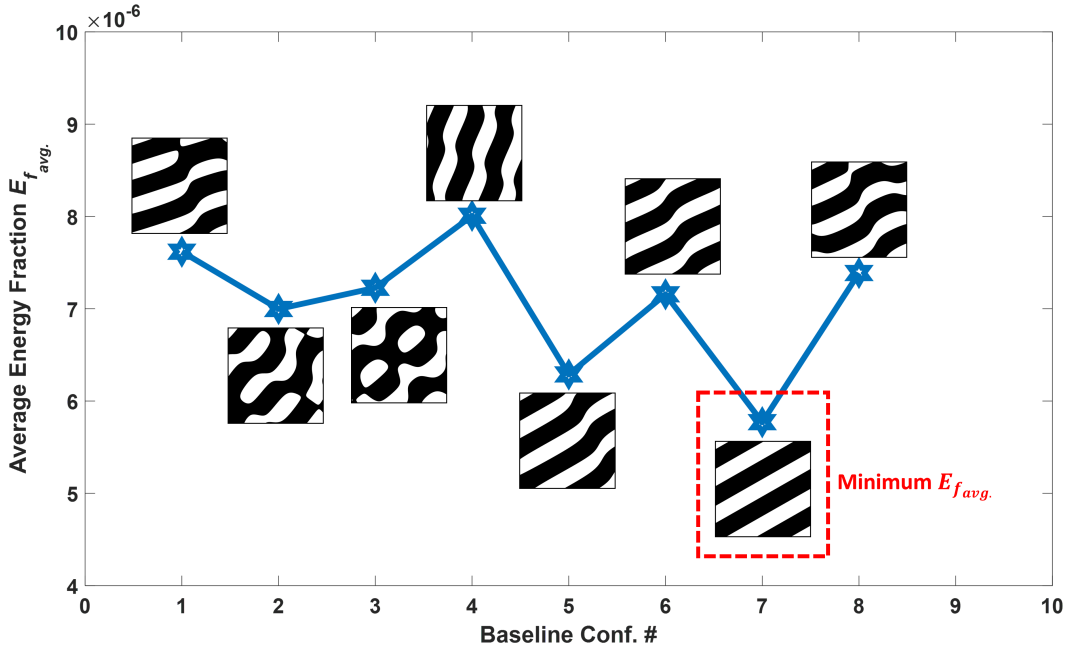

Fig. 6 Baseline spinodal designs.

$E_{f_{avg.}}$ values of each design are determined according to this threshold value. $E_{f_{avg.}}$ stands for the average of energy fractions above the threshold. The elemental energy fraction values of the set of designs are depicted in Fig. 7.

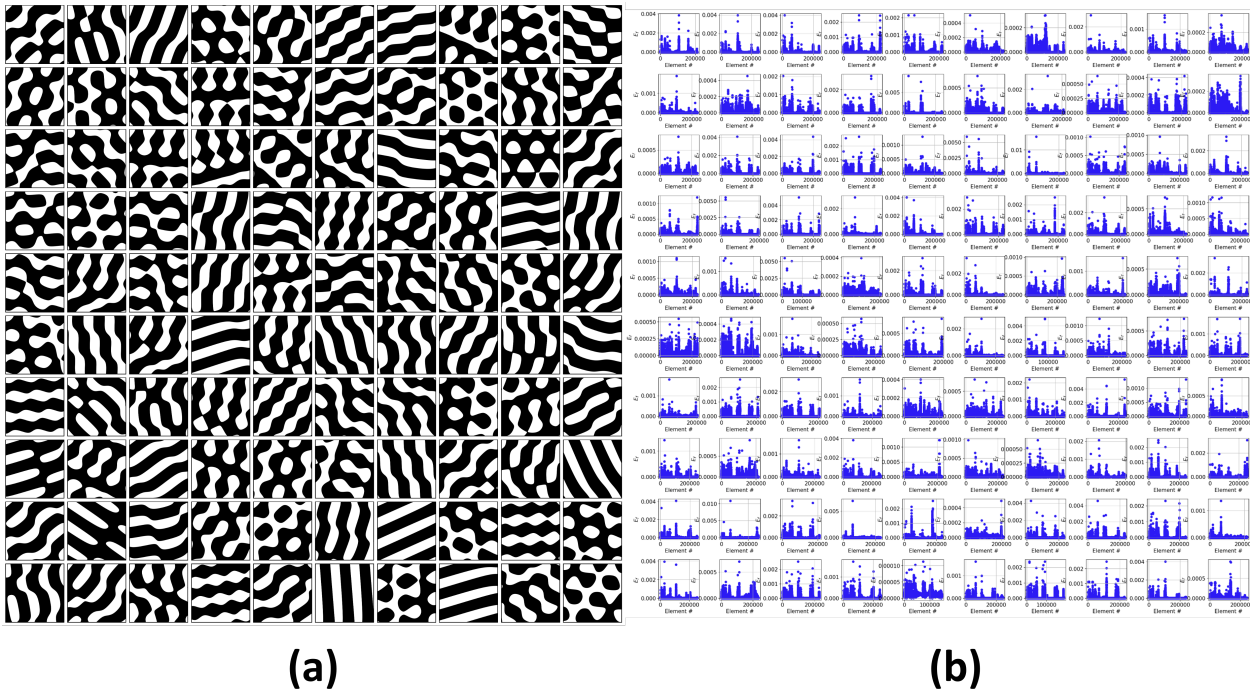

Fig. 7 Energy fraction of the example data samples (a) spinodal topologies, (b) energy fraction results.

Data collection for the surrogate model begins with recording simulation inputs (η_m parameters) and outputs (maximum and average E_f values). To compute the average E_f, only values above a threshold set by the baseline design are included. Out of the 400 data points generated, 300 are used for training, with 50 each reserved for validation and testing. Data generation takes approximately 1.1231e+05 seconds on a cluster using an AMD EPYC 7702 CPU at 3.35 GHz, covering spinodal material simulations.

Through architecture tuning, a three-layer feedforward neural network with 128 neurons per layer, ReLU activation, and 10 % dropout is selected. Larger configurations demonstrate no accuracy gains while reducing layer size increases training time. With a compact feature set of 8 inputs and 2 outputs, training is fast, finishing in a few seconds. Due to the high discrepancy in the maximum output of the data, log scaling is applied apart from normalization. The model's mean absolute error (MAE) is nearly identical between validation and test sets, with MAE values of 9.47 %. Fitting accuracy for average E_f outperforms that for the maximum as shown in Fig. 8, likely due to mesh limitations that can lead to abrupt changes in peak values [21].

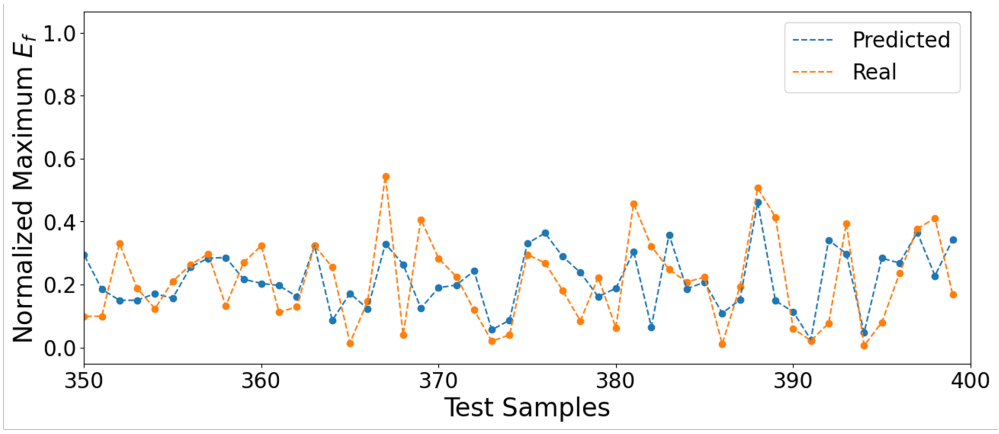

(a)

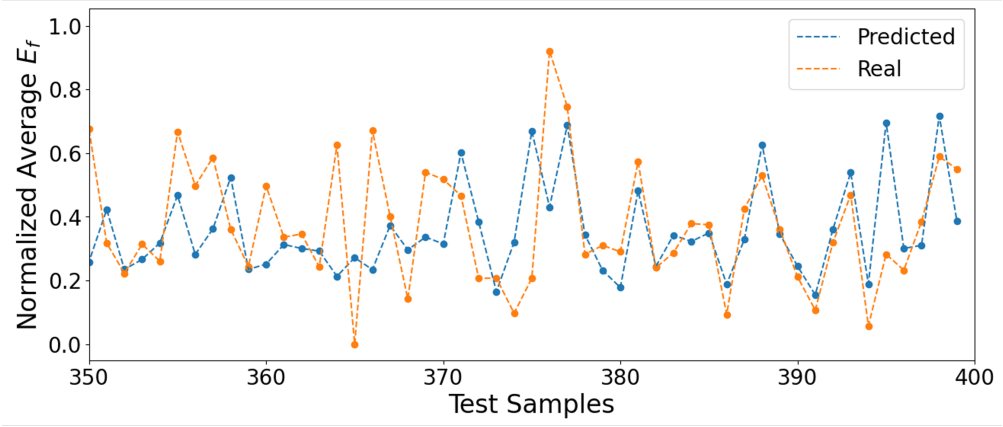

(b)

Fig. 8 Performance of the surrogate model on the test data for (a) maximum (b) average E_f.

Despite limited data preventing further MAE reduction, this surrogate model provides a fast and practical alternative for iterative design, as illustrated by the close alignment between predicted and observed values for both maximum and average E_f in Fig. 9.

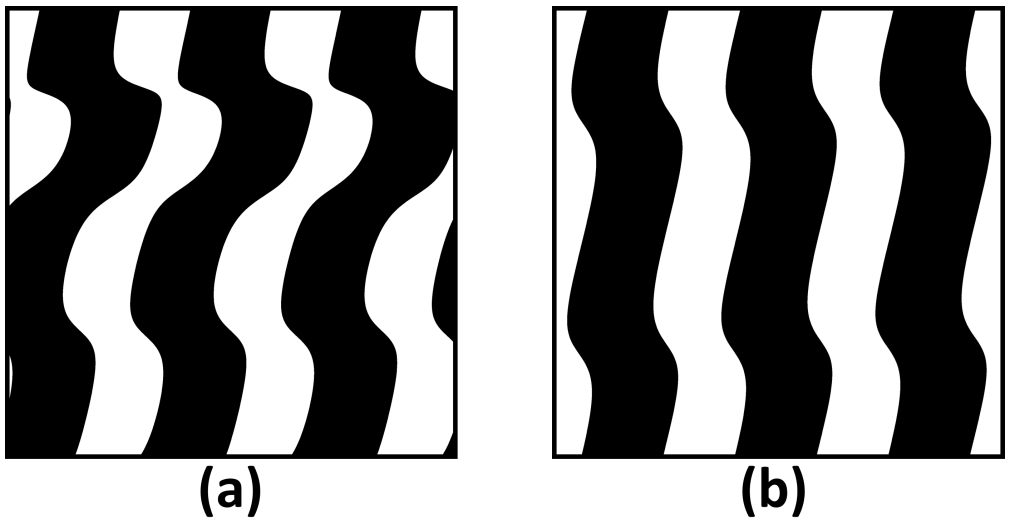

Fig. 9 (a) DL-based and (b) conventional optimization results

B. Comparison with conventional truss-based metamaterials

The mechanical performance of the spinodal metamaterials under static loading is compared with the truss-based metamaterials, which are selected as the common configurations such as simple-cubic (SC), body-centered-cubic (BCC), face-centered-cubic (FCC), face-body-centered-cubic (FBCC), diamond-cubic (DC), and face-body-centered-diamond-cubic (FBCDC). The same relative density (60%) is utilized for all configurations ensuring a fair comparison. The main idea behind this comparison is to demonstrate the mechanical performance improvement achieved by spinodal metamaterials over conventional truss-based metamaterials for a linear elastic behavior. The selected truss-based configurations are designed using the same frame size, which is 1% of the side length. The six different types of 2D truss-based metamaterial geometries are given in Fig. 10.

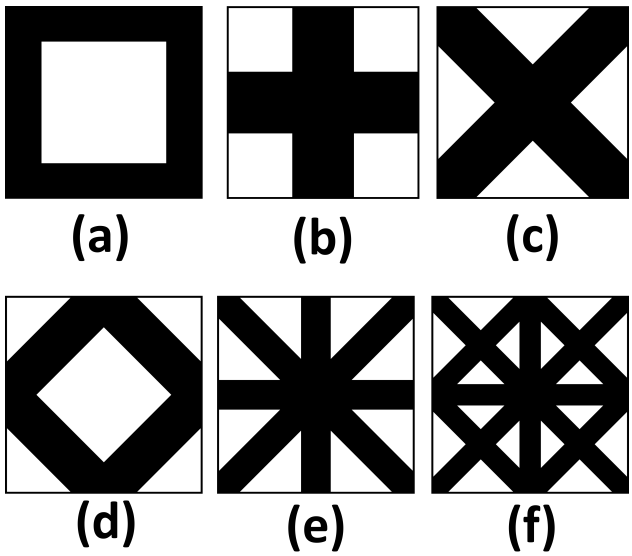

Fig. 10 Conventional truss-based metamaterials (a) SC (b) BCC, (c) FCC, (d) DC, (e) FBCC, (f) FBCDC.

The DL-based and physics-based optimization are conducted to obtain the optimum spinodal configuration as explained in Section 3A. Next, the performance of optimum spinodal topology is compared with conventional lattice

structures. The objective function, which is given in Eq. (7) is selected as performance criteria as given in Fig. 11.

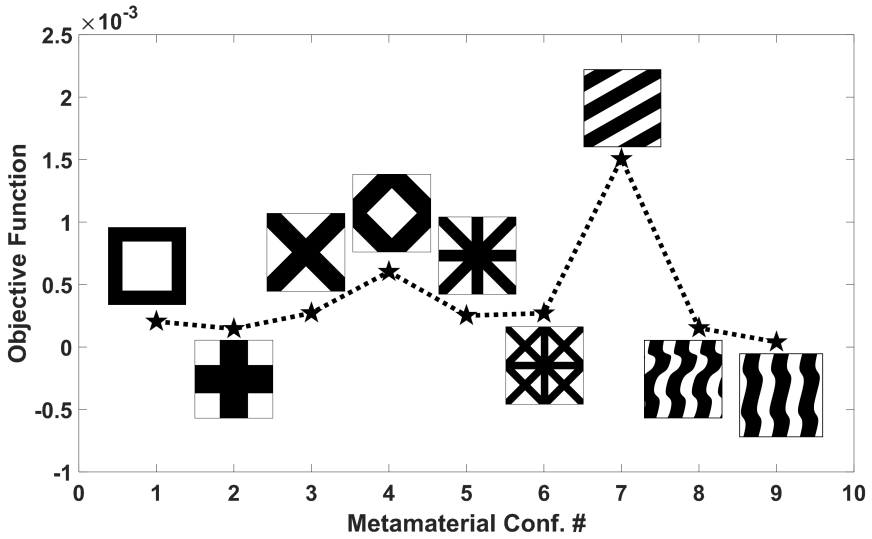

Fig. 11 Objective function comparison for truss-based and spinodal metamaterials.

The optimum spinodal metamaterial of the DL-based solution shows a relatively low energy fraction value in comparison to conventional truss-based materials except for BCC. The main reason why BCC performs slightly better than the optimal spinodal material is that the BCC uses the merits of both vertical and horizontal trusses with high thickness, which improves the response under both shear and tension. On the other hand, the optimum spinodal metamaterial of the physics-based solution shows impressive behavior, which results in the lowest objective function. However, the performance of the DL-based method can be improved using more data points. The worst performance in terms of energy fraction is observed for the baseline spinodal configuration, where the trusses are aligned with 45^o. For this respect, enhancement in energy fractions relative to the baseline model for all metamaterial configurations, including the optimal spinodal design, is listed in Table 3.

Table 3 Improvement in mechanical behavior for all configurations relative to the baseline configuration.

Metamaterial	Improvement (%)
SC	86.4%
BCC	90.3%
FCC	82%
DC	60%
FBCC	83.3%
FBCDC	82%
DL-based Optimal Spinodal Design	89.8%
Conventional Optimal Spinodal Design	97.4%

As seen from Table 3., both DL-based and physics-based frameworks identify optimal spinodal metamaterial designs demonstrating relatively low stress/strain concentrations in comparison to the baseline model and most of the conventional truss-based metamaterials. While the optimum design of the physics-based solution reveals the best performance increment compared to the baseline design (97.4%), the DL-based solution demonstrates 89.8% enhancement, which is approximately the same as the performance of the BCC material. The smallest enhancement is obtained for the DC lattice. The other truss-based metamaterials demonstrate up to 15.4% lower performance improvement in comparison to the optimal design.

The stress and strain components are depicted for optimal spinodal, FCC, and FBCDC designs as contour plots in Fig. 12.

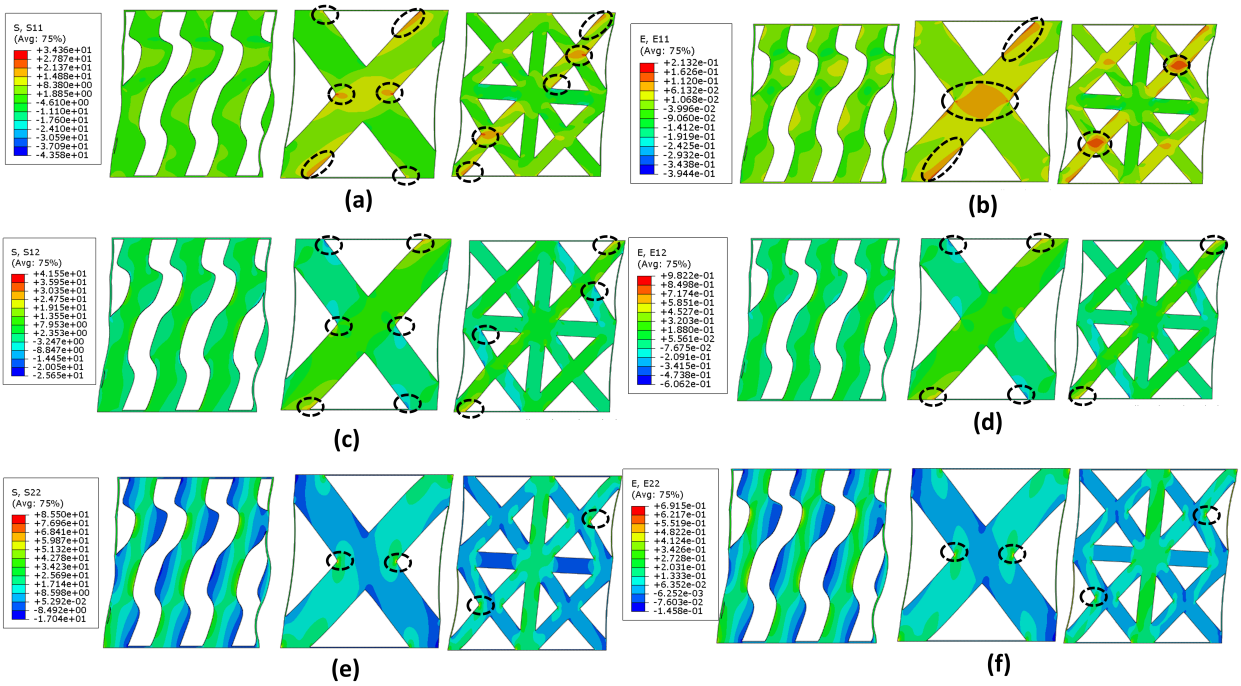

Fig. 12 Stress and strain comparison as FEA contour plots for optimum spinodal, FCC, and FBCDC designs (a) σ_{11} (b) ε_{11} (c) σ_{12}, (d) ε_{12}, (e) σ_{22}, (f) ε_{22}.

It is clearly seen from Fig. 12 that the truss-based lattices demonstrate higher stress and strain concentrations due to their sharp connections in comparison to smooth geometries of spinodal materials.

IV. Conclusion

In this study, metallic spinodal metamaterials are modeled using a GRF-based formulation. A large number of design sets are generated, where the orientation distribution arrays define the topology of each spinodal configuration. The optimization is performed using the physics-based and DL-based approaches to determine the optimal spinodal geometry providing the lowest average and maximum energy fractions, which are calculated through numerical simulations. Furthermore, the mechanical behavior of the optimal spinodal metamaterial design is compared with conventional truss-based metamaterials showing high-stress concentrations. The main findings of this study are as follows:

- A computationally efficient DL-based surrogate model using the FNN method is developed for fast optimization of 2D spinodal materials with reasonable accuracy for the first time in literature.
- Energy fraction, which is picked as an objective of the optimization framework, is a compact metric for elemental stress/strain responses.
- The computing costs of the FEA-based optimization can be minimized with the use of the DL-based strategy.
- The optimum spinodal design demonstrates up to 37.4% enhancement compared to truss-based metamaterials.
- The proposed DL-based model can further be improved using more data samples. Furthermore, the optimum design of the DL-based model can be used as the initial design of the mathematical optimization framework involving the FE simulations to reduce high computational costs.

The aforementioned findings support the potential use of spinodal metamaterials in aerospace systems. The future work will focus on 3D modeling and design of spinodal metamaterials.

Acknowledgments

The authors express their thanks to Dr. Sheng Liu for the development of prior studies on spinodal metamaterials. The authors would like to acknowledge the financial support from the National Science Foundation CAREER Award CMMI-2236947, AFOSR Award BAA FA9550-23-S-0001, and the Future Additive Interdisciplinary Manufacturing (FAIM) project supported under the National Defense Education Program of the Office of Naval Research (ONR).

References

[1] Fan, J., Zhang, L., Wei, S., Zhang, Z., Choi, S.-K., Song, B., and Shi, Y., "A review of additive manufacturing of metamaterials and developing trends," *Materials Today*, Vol. 50, 2021, pp. 303–328.

[2] Gibson, L. J., Ashby, M. F., Schajer, G., and Robertson, C., "The mechanics of two-dimensional cellular materials," *Proceedings of the Royal Society of London. A. Mathematical and Physical Sciences*, Vol. 382, No. 1782, 1982, pp. 25–42.

[3] Kumar, S., Tan, S., Zheng, L., and Kochmann, D. M., "Inverse-designed spinodoid metamaterials," *npj Computational Materials*, Vol. 6, No. 1, 2020, p. 73.

[4] Grant, C. P., "Spinodal decomposition for the Cahn-Hilliard equation," *Communications in Partial Differential Equations*, Vol. 18, No. 3-4, 1993, pp. 453–490.

[5] Zheng, L., Kumar, S., and Kochmann, D. M., "Data-driven topology optimization of spinodoid metamaterials with seamlessly tunable anisotropy," *Computer Methods in Applied Mechanics and Engineering*, Vol. 383, 2021, p. 113894.

[6] Mao, Y., Yang, Z., Jha, D., Paul, A., Liao, W.-k., Choudhary, A., and Agrawal, A., "Generative adversarial networks and mixture density networks-based inverse modeling for microstructural materials design," *Integrating Materials and Manufacturing Innovation*, Vol. 11, No. 4, 2022, pp. 637–647.

[7] Röding, M., Wåhlstrand Skärström, V., and Lorén, N., "Inverse design of anisotropic spinodoid materials with prescribed diffusivity," *Scientific Reports*, Vol. 12, No. 1, 2022, p. 17413.

[8] Golnary, F., and Asghari, M., "Data-driven analysis of spinodoid topologies: anisotropy, inverse design, and elasticity tensor distribution," *International Journal of Mechanics and Materials in Design*, 2024, pp. 1–23.

[9] Thakolkaran, P., Espinal, M. A., Dhulipala, S., Kumar, S., and Portela, C. M., "Experiment-informed finite-strain inverse design of spinodal metamaterials," *arXiv preprint arXiv:2312.11648*, 2023.

[10] Vafaeefar, M., Moerman, K. M., Kavousi, M., and Vaughan, T. J., "A morphological, topological and mechanical investigation of gyroid, spinodoid and dual-lattice algorithms as structural models of trabecular bone," *Journal of the Mechanical Behavior of Biomedical Materials*, Vol. 138, 2023, p. 105584.

[11] Wojciechowski, B., Xue, Y., Rabbani, A., Bolton, J. S., and Sharma, B., "Additively manufactured spinodoid sound absorbers," *Additive Manufacturing*, Vol. 71, 2023, p. 103608.

[12] Vafaeefar, M., Moerman, K. M., and Vaughan, T. J., "Experimental and computational analysis of energy absorption characteristics of three biomimetic lattice structures under compression," *Journal of the Mechanical Behavior of Biomedical Materials*, Vol. 151, 2024, p. 106328.

[13] Gorguluarslan, R. M., Gungor, O. U., Yıldız, S., and Erem, E., "Energy absorption behavior of stiffness optimized graded lattice structures fabricated by material extrusion," *Meccanica*, Vol. 56, 2021, pp. 2825–2841.

[14] Liu, S., and Acar, P., "Generative Adversarial Networks for Inverse Design of Two-Dimensional Spinodoid Metamaterials," *AIAA Journal*, 2024, pp. 1–10.

[15] Torczon, V., "On the convergence of pattern search algorithms," *SIAM Journal on optimization*, Vol. 7, No. 1, 1997, pp. 1–25.

[16] Ramesh, A., Pavlov, M., Goh, G., Gray, S., Voss, C., Radford, A., Chen, M., and Sutskever, I., "Zero-shot text-to-image generation," *International conference on machine learning*, Pmlr, 2021, pp. 8821–8831.

[17] Soyarslan, C., Bargmann, S., Pradas, M., and Weissmüller, J., "3D stochastic bicontinuous microstructures: Generation, topology and elasticity," *Acta materialia*, Vol. 149, 2018, pp. 326–340.

[18] Chen, Q., and Thouas, G. A., "Metallic implant biomaterials," *Materials Science and Engineering: R: Reports*, Vol. 87, 2015, pp. 1–57.

[19] Bartolomeu, F., Costa, M., Alves, N., Miranda, G., and Silva, F. S., "Selective Laser Melting of Ti6Al4V sub-millimetric cellular structures: Prediction of dimensional deviations and mechanical performance," *journal of the mechanical behavior of biomedical materials*, Vol. 113, 2021, p. 104123.

[20] Jiexian, M., "Im2mesh (2D image to triangular meshes)(https://www. mathworks. com/matlabcentral/fileexchange/71772-im2mesh-2d-image-to-triangular-meshes)," *MATLAB Central File Exchange*, 2021.

[21] Zienkiewicz, O. C., and Taylor, R. L., *The finite element method set*, Elsevier, 2005.